Journal of Alzheimer's Disease 31 (2012) S87–S99
DOI 10.3233/JAD-2012-112072
IOS Press

Research Report

Proton and Phosphorus Magnetic Resonance Spectroscopy of a Mouse Model of Alzheimer's Disease

Vladimír Mlynárik[a,*], Matthias Cacquevel[b], Lili Sun-Reimer[a], Sharon Janssens[a], Cristina Cudalbu[a], Hongxia Lei[a], Bernard L. Schneider[b], Patrick Aebischer[b] and Rolf Gruetter[a]
[a]*Ecole Polytechnique Fédérale de Lausanne, Laboratory of Functional and Metabolic Imaging (LIFMET), Lausanne, Switzerland*
[b]*Ecole Polytechnique Fédérale de Lausanne, Brain Mind Institute, Lausanne, Switzerland*

Accepted 29 February 2012

Abstract. The development of new diagnostic criteria for Alzheimer's disease (AD) requires new *in vivo* markers reflecting early pathological changes in the brain of patients. Magnetic resonance (MR) spectroscopy has been shown to provide useful information about the biochemical changes occurring in AD brain *in vivo*. The development of numerous transgenic mouse models of AD has facilitated the evaluation of early biomarkers, allowing researchers to perform longitudinal studies starting before the onset of the pathology. In addition, the recent development of high-field animal scanners enables the measurement of brain metabolites that cannot be reliably quantified at lower magnetic fields. In this report, we studied a new transgenic mouse model of AD, the 5xFAD model, by *in vivo* proton and phosphorus MR spectroscopy. This model, which is characterized by an early-onset and a robust amyloid pathology, developed changes in the neurochemical profile, which are typical in the human disease, i.e., an increase in myo-inositol and a decrease in N-acetylaspartate concentrations, as early as in the 40th week of age. In addition, a significant decrease in the γ-aminobutyrate concentration was observed in transgenic mice at this age compared to controls. The pseudo-first-order rate constant of the creatine kinase reaction as well as relative concentrations of phosphorus-containing metabolites were not changed significantly in the 36 and 72-week old transgenic mice. Overall, these results suggest that mitochondrial activity in the 5×FAD mice is not substantially affected but that the model is relevant for studying early biomarkers of AD.

Keywords: 5xFAD, Alzheimer's disease, *in vivo* NMR spectroscopy, metabolic profile, transgenic mice

INTRODUCTION

Transgenic mouse models of Alzheimer's disease (AD) are useful for studying disease mechanisms and for therapy testing. The design of such models has been based on the early discovery of dominant mutations in rare familial AD cases (FAD) [1–3] and in familial fronto-temporal dementia cases linked to chromosome 17 (FTDP-17) [4]. Most of transgenic mouse models of AD are based on the overexpression of mutated forms of human amyloid-β protein precursor (AβPP) alone or in combination with mutated human presenilin 1 (PS1) or 2 (PS2) genes (see [5] for an extensive review of transgenic mouse models of AD). These models are characterized by a progressive accumulation of amyloid-β (Aβ) in the brain, which leads to the age-dependent formation of extracellular amyloid deposits, one of the neuropathological hallmark of AD.

*Correspondence to: Vladimír Mlynárik, PhD, Laboratory of Functional and Metabolic Imaging, Station 6, 1015 Lausanne, Switzerland. Tel.: +41 21 6937685; Fax: +41 21 6937960; E-mail: vladimir.mlynarik@epfl.ch.

ISSN 1387-2877/12/$27.50

Although these transgenic mice reproduce well subsets of histopathological features typical for AD, most of them do not show the complete phenotype of AD including neurofibrillary tangles and massive neuronal loss. To overcome these limitations, double or triple transgenic mouse models overexpressing the human tau gene carrying FTDP-17 mutations together with mutated AβPP and/or PS1/2 have been generated with various neuropathological outcomes [6, 7]. However, despite these efforts, none of these models recapitulates the full spectrum of the disease. Therefore, each mouse model has to be critically evaluated and compared to the human disease in order to assess its relevance to AD [8, 9].

Neurochemical profile in AD patients

In vivo magnetic resonance spectroscopy (MRS) is a non-invasive method, which provides information on the neurochemical profile in various neurodegenerative diseases. This method enables studying various brain metabolites in a defined volume of interest (VOI) that can cover brain regions as small as 1 milliliter in human brain and several microliters in rodents [10]. It can be used in human neurological patients as well as in animals modeling various brain pathologies.

Proton (^{1}H) MR spectroscopy is capable of providing relative or absolute concentrations of about 15 to 19 metabolites in the brain. Some of them are considered markers of myelination and cell proliferation such as phosphorylcholine, glycerophosphorylcholine, and phosphoethanolamine because they are precursors of essential structural components of the plasma membrane (phospholipids) and the myelin sheath (sphingolipids). Others, such as creatine (Cr), phosphocreatine (PCr), glucose, lactate, and alanine, are related to energy metabolism. Taurine and *myo*-inositol (mIns) are osmoregulators; they are notably involved in calcium signaling. Glutamate (Glu), glutamine (Gln), γ-aminobutyrate (GABA), aspartate, and glycine are involved in neurotransmitter metabolism; glutathione and ascorbate are antioxidants. N-acetylaspartate (NAA) has various biological functions (osmoregulation, energy metabolism, myelinization) and is mainly produced by the mitochondria of neurons in the brain.

Phosphorus (^{31}P) MR spectroscopy has lower sensitivity than ^{1}H MR spectroscopy and requires larger VOIs to be measured [11]. The most important cerebral metabolites that can be measured by ^{31}P spectroscopy are nucleotide triphosphates, mainly adenosine triphosphate (ATP), which is the principal energy source for cell metabolism, and PCr, which serves as an ATP replenisher via the creatine kinase reaction. Other peaks seen in the ^{31}P brain spectra can be assigned to phosphomonoesters (PME) consisting of poorly resolved signals of phosphoethanolamine and phosphorylcholine, to inorganic phosphate (Pi), to phosphodiesters (PDE) consisting of peaks of glycerophosphorylethanolamine and glycerophosphorylcholine, and to nicotinamide adenine dinucleotide and its phosphate (NAD+NADP). PME and PDE are precursors and breakdown products, respectively, of membrane phospholipids; Pi is a product of ATP hydrolysis; and NAD and NADP are involved in redox reactions. It should be noted that the role of many metabolites detected by ^{1}H or ^{31}P spectroscopy is not completely clear and some of them have multiple roles.

Changes in concentrations of several brain metabolites were reported in AD patients. In particular, a decrease in the concentration of NAA and an increase in mIns were consistently found not only in patients with clinical symptoms of AD but also in people with the syndrome of mild cognitive impairment, which present a higher risk to develop AD [12].

NAA is considered a marker of neuronal functionality and integrity and its concentration is decreased in both grey and white matter of the AD patients [13–17]. Moreover, the decrease in NAA demonstrating gradual neuronal loss was found to correlate with severity of neuropathological findings [18, 19]. In contrast, mIns is believed to be a marker of glial cell numbers because it is highly concentrated in astrocytes. The concentration of this metabolite is elevated in grey matter even in the earliest stages of AD [20], probably due to gliosis.

There are other metabolites easily detectable in MR spectra of human brain. The peak of total choline corresponds mainly to phosphorylcholine and glycerophosphorylcholine. The changes in the total choline concentration are probably associated with increased membrane turnover due to neurodegeneration. The reports on the choline concentration in AD are contradictory. Various authors found increased [21, 22] or decreased [23, 24] total choline levels in some brain regions, whereas most studies reported no change in its concentration [25–27].

The methyl peak of total creatine (tCr) is composed of PCr and Cr. The PCr/Cr system acts as a source of energy reserve for neurons and glial cells. An unchanged concentration of tCr was assumed in most human and animal MR studies and concentrations of other metabolites were generally expressed as relative ones, i.e., as ratios to tCr. However, a decrease [24, 28], as well as an increase [20], in tCr has also been reported in AD.

Glu is a key excitatory neurotransmitter. It can be quantified in human brain at higher static magnetic fields separately from Gln. At lower magnetic fields, a sum of Glu and Gln concentrations (Glx) is usually obtained. In AD patients, a decrease of Glx or Glu was reported in the occipital cortex [16], the frontal lobe [29], the posterior cingulate [30], and in the hippocampus [27], respectively.

Lactate is a product of anaerobic glycolysis. The peak of lactate can be seen in spectra of human brain in disorders connected with hypoxia.

Neurochemical profile in AD transgenic mouse models

Several types of AD mouse models were studied by MRS (see [31] for an excellent review). Tg2576, a single-transgenic mouse model overexpressing the human AβPP carrying the *Swedish* mutation (K670N, M671L) develops amyloid plaques predominantly in the neocortex and the hippocampus by 10–16 months of age [32]. In this model, a decrease of NAA, Glu, and glutathione concentrations and an increase in taurine was found in the cerebral cortex at 19 months of age [33]. A decreased level of NAA is consistent with decreased neuronal viability. The authors proposed that the role of taurine in rodent brain might be similar to that of mIns in human brain, and that an increased level of taurine could reflect increased glial volume.

The Tg2576 model was crossed with a transgenic mouse overexpressing mutated human PS1 (M146L) and double transgenic animals (AβPP/PS1) showed accelerated amyloid deposition [34]. Oberg and colleagues [35] measured MR spectra in hippocampus of these mice at 2.5, 6.5, and 9 months of age. The first plaques were seen at 6.5 months and statistically significant lower relative concentrations of NAA, Glu, and a macromolecule component at 1.2 ppm were observed at 9 months of age. Another MRS study on the same transgenic model was conducted by Marjanska et al. [36, 37]. At 16, 20, and 23 months of age, they found that the levels of NAA and Glu decreased, and the level of mIns increased with animal aging. At 16 months, the levels of NAA and Glu were lower and the mIns level was higher than the corresponding levels observed in the wild-type animals. Interestingly, an increase in taurine concentration similar to that observed in the Tg2576 mice was not seen.

A rather similar AβPP/PS1 mouse model was studied by Choi et al. [38]. This model was generated by crossing the Tg2576 mice with another transgenic line overexpressing mutated human PS1 (M146V) [38, 39]. They measured proton spectra in cortex and hippocampal regions at 6 and 16–18 months of age. At 6 months of age, a small plaque accumulation was observed with no significant changes in the neurochemical profile compared to wild-type controls. At 16–18 months, a large plaque burden was accompanied by a decrease in NAA and Glu and by an increase of Gln and mIns concentrations (*in vitro*, as μmol/g wet weight) in cortex. However, only a decrease in NAA was seen *in vivo* at 17–20 months of age in the hippocampus. In the same study, the effect of anti-inflammatory drugs on MR spectroscopic changes in AβPP/PS1 mice was also assessed. Ibuprofen treatment reverted the decrease in NAA and Glu, and celecoxib reverted the decrease in NAA.

Chen and co-workers [40] studied another AβPP/PS1 mouse model, with human PS1 carrying the ΔE9 mutation [41–44], at 3, 5, and 8 months of age. Surprisingly and contrary to previous observations on other AβPP/PS1 mice, they found a very early increase in mIns/tCr in both the hippocampus and the cortex at the age of 3 months and a decrease in NAA/tCr at the age of 5 months. Changes in relative concentrations of both metabolites progressed with age.

Brain metabolites changes were also studied in another double transgenic mouse model of AD, the so-called PS2AβPP line, which overexpresses the mutant AβPP (K670N, M671L) and human PS2 (N141I) genes [45]. In frontal cortex of 24-month old animals a significant decrease in NAA/tCr and Glu/tCr was observed compared to wild-type mice while no significant change in mIns/tCr was observed at this time point [46]. These spectroscopic changes correlated with the amount of plaques in the frontal cortex. A summary of metabolic changes in mouse models of amyloid pathology measured by *in vivo* proton MR spectroscopy is given in Table 1.

Recently, two other transgenic models were studied. In the first, triple-transgenic model (3xTg-AD) harboring PS1 (M146V), AβPP (K670N, M671L), and tau (P301L) transgenes [6], a decrease in NAA and taurine and an increase in lactate concentrations were observed in hippocampus at 3 and 15 months of age [47]. In an earlier study of this model, a decline in NAA was observed in hippocampus at 6 months of age [48]. In the second model, a transgenic mouse overexpressing the tau gene carrying the P301L mutation [49], which develops neurofibrillary tangles and present an early neurodegeneration, a decrease in taurine and also NAA and Glu was seen in hippocampus and olfactory bulb, respectively, at 5 months of age [50]. In

Table 1
Summary of metabolic changes measured in mouse models of amyloid pathology by *in vivo* proton MR spectroscopy

Strain	Transgene	Promoter	Kinetics of amyloid deposition[a] (months)	Age of MRS analysis (months)	VOI position and size	Neuropathology in the VOI[b]	Main metabolite changes[c]
Tg2576 [32, 66, 67]	Human $A\beta PP_{695}$ with *Swedish* mutation (K670N/M671L)	Hamster PrP	6–7, 12, ≥19	19 [33]	Neocortex fronto-parietal $6 \times 2 \times 3\,mm^3$	Sparse amyloid deposition with large amyloid plaques and plaque associated gliosis	↑Tau[d] ↓NAA, GSH, Glu[d]
AβPP/PS1[e] (Tg2576 $\times PS1_{M146L}$) [34, 39, 68]	Human $A\beta PP_{695}$ with *Swedish* mutation (K670N/M671L) × Human PS1 with M146L mutation	Hamster PrP for AβPP × PDGFβ2 for PS1	4, 6, ≥9	2.5, 6.5, 9 [35]	Dorsal hippocampus $2 \times 2 \times 2\,mm^3$	No pathology at 2.5 months. Presence of few amyloid deposits at 6.5 with a small increase at 9 months	↓NAA/tCr ↓Glu/tCr ↓M1.2/tCr[f] (6.5–9 months)
				16, 20, 23 [36]	Dorsal hippocampus and cortex $18\,mm^3$	n/a	↓NAA/tCr (with age) ↓Glu/tCr (with age) ↑mIns/tCr (20 months)
AβPP/PS1[e] (Tg2576 $\times PS1_{M146V}$) [38, 39]	Human $A\beta PP_{695}$ with *Swedish* mutation (K670N/M671L) × Human PS1 with M146V mutation	Hamster PrP for AβPP × PDGFβ2 for PS1	4, 6, ≥9	6, 16–20 [38]	Frontal cortex and hippocampus (subiculum) $2 \times 2.2 \times 2\,mm^3$	Significant plaque number at 6 months, large burden at 16–18 months in the frontal cortex	↓NAA, Glu ↑mIns, Gln in cortexd (16–18 months) ↓NAA/tCr in hippocampus (17–20 months)
AβPP/PS1 line 85[g] [41–44]	Chimeric mouse/human $A\beta PP_{695}$ with *Swedish* mutation (K670N/M671L) & Human PS1 with ΔE9 mutation	Mouse PrP for both transgenes	4–6, 9, ≥12	3, 5, 8 [40]	Dorsal hippocampus and adjacent cortex	No amyloid plaques at 3 months. Sparse amyloid deposition at 5 months	↑mIns/tCr (3–8 months, with age) ↓NAA/tCr (5–8 months, with age)
PS2AβPP[e] [45]	Human $A\beta PP_{751}$ with *Swedish* mutation (K670N/M671L) × Human PS2 with N141I mutation	Thy1.2 for AβPP × Mouse PrP for PS2	5–6, 9, ≥13	4–24 [46]	Frontal cortex $1.5 \times 1.7 \times 3.4\,mm^3$	High content of amyloid pathology at 23 months. Correlation between plaque load and metabolites changes	↓NAA/tCr ↓Glu/tCr (20, 24 months)
5×FAD[g] (Tg6799) [52, 62]	Human $A\beta PP_{695}$ with *Swedish* (K670N/M671L), *Florida* (I716 V), *London* (V717I) mutations & Human PS1 with M146L and L286 V mutations	Thy1 promoter for both transgenes	1.5–2, 2–3, ≥4	9, 10, 11 this work	Dorsal hippocampus $1.2 \times 1.9 \times 1.9\,mm^3$	High amount of amyloid plaques with massive gliosis	↓NAA ↓Glu (9 months) ↓NAA ↓GABA ↑mIns (10,11 months)

[a]Numbers denote the age (in months) of three stages of amyloid deposition, onset, mild and severe amyloid deposition, respectively. [b]Neuropathology in the VOI as described in the MR study. [c]Significant differences between wild-type and transgenic animals at a particular age (trends in age are also indicated). [d]*In vitro* data, differences in the values *in vivo* were not significant. [e]Two different strains were breed to generate this mouse model. [f]M1.2 denotes a signal of macromolecules at 1.2 ppm. [g]Both transgenes were integrated at the same locus. GABA, γ-aminobutyrate; Gln, glutamine; Glu, glutamate; GSH, glutathione; mIns; *myo*-inositol; MRS, magnetic resonance spectroscopy; NAA, N-acetylaspartate; tCr, total creatine; VOI, volume of interest.

the same model, Yang and collaborators [51] observed an increase in mIns/tCr in transgenic mice compared to wild-type controls at 5 and 8 months of age, however, no significant change in NAA/tCr was observed at these time points.

Besides the decrease in NAA, the other typical change of the neurochemical profile in the human AD brain, i.e., the increase in mIns, was observed only in elderly AβPP/PS1 mice. In attempt to find a transgenic model showing the neurochemical profile closer to the human one in younger animals, a 5xFAD transgenic mouse model was used in the present study. Localized ^{1}H spectra in brain of these transgenic mice were measured at 36–44 weeks of age and their metabolic profiles were compared to those of wild-type animals. Furthermore, ^{31}P MR spectra providing additional information on cell energy metabolism were measured from brains of the transgenic and wild-type mice. Relative concentrations of phosphorus-containing metabolites in the brain were evaluated, and the pseudo-first order forward rate constants k_{for} of the creatine kinase reaction (PCr $\leftrightarrow$ ATP) were obtained by localized phosphorus saturation transfer experiment. Spectroscopic results were compared with histology.

MATERIALS AND METHODS

Animal model

The 5xFAD mouse line was generated in the laboratory of Dr. Robert Vassar at Northwestern University, Chicago [52] and was transferred to our institute from Jackson Laboratories, US (Stock number: 006554). This transgenic line overexpresses both the AβPP and the PS1 genes, carrying familial AD (FAD) mutations: AβPP K670N/M671L (*Swedish*), I716V (*Florida*), and V717I (*London*); PS1 M146L and L286V. Both transgenes are driven by the Thy1 promoter. Animals were maintained on a mix genetic background (C57/B6SJL) and wild-type littermates were use as controls mice. All procedures were approved by the Committee on Animal Experimentation for the canton of Vaud, Switzerland, in accordance with Swiss Federal Laws on Animal Welfare and the European Community Council directive (86/609/EEC) for the care and use of laboratory animals.

MR spectroscopy

Seven AD and seven wild-type mice anesthetized with 1–2% isoflurane were measured at the age of 36 weeks (^{31}P and ^{1}H spectra), 40 and 44 weeks (^{1}H only), and 72 weeks (^{31}P only). Measurements were conducted on a 14.1 T/26 cm horizontal-bore Varian VNMRS scanner (Varian, Palo Alto, CA, USA). The magnet was equipped with 12-cm inner-diameter actively shielded gradient sets (Magnex Scientific, Oxford, UK) allowing a maximum gradient of 400 mT/m in 120 μs. For ^{1}H spectroscopy, a two-loop quadrature radiofrequency coil with dimensions of 21 mm × 14 mm was used as a transceiver. The static field homogeneity was adjusted using first- and second-order shims using an EPI version of FASTMAP [53].

Localizer images were obtained in the coronal plane using a multislice turbo-spin-echo protocol (TR/TE_{eff} = 5000/52 ms, echo train length = 8, field-of-view = 24 mm × 24 mm, slice thickness = 0.6 mm, 6 averages, 128^2 image matrix). The MRI scan was followed by short echo-time (TR/TE = 4000/2.8 ms) spin echo, full intensity acquired localized (SPECIAL) [54] proton MR spectroscopy from volumes of interest of $1.2 \times 1.9 \times 1.9\,mm^3$ centered in dorsal hippocampus and of $1.7 \times 1.5 \times 1.7\,mm^3$ centered in its temporal pole. Outer volume suppression was used, which was interleaved with water signal suppression by variable-power RF pulses with optimized relaxation delays (VAPOR) [55]. Each scan of 4096 complex data points was acquired with a spectral width of 7 kHz. Proton spectra were quantified by LCModel [56] using a database of simulated spectra of metabolites together with an experimental spectrum of macromolecules measured in a healthy mouse brain [57]. Absolute concentrations of metabolites in μmol/g of tissue were calculated using an unsuppressed water peak, assuming 80% of water in the tissue.

^{31}P spectra and saturation transfer data were measured using a dual surface radiofrequency coil consisting of a proton quadrature coil and a linearly polarized 10 mm diameter phosphorus coil, both used as transceivers. The localization pulse sequence consisted of outer volume saturation (OVS) using 2.5 ms hyperbolic secant pulses. Afterwards, one-dimensional ISIS [58] localization was used in the horizontal direction. It consisted of a 2.5 ms hyperbolic secant pulse inverting the magnetization in the selected region of brain in alternate scans, which was followed by a 1 ms broadband nonselective adiabatic half passage pulse and a signal acquisition with alternated phase. The repetition time was 4 seconds.

In the saturation transfer experiment, the γ-ATP signal was saturated by a BISTRO pulse train [59] interleaved with OVS. The BISTRO pulse sequence consisted of a series of 40 ms hyperbolic secant pulses

with variable amplitudes and having a total length t_{sat} from 0.324 s to 3.24 s. Sixty to eighty scans were collected for each of 6 different saturation times and for a control scan with irradiation offset in the mirror position relative to the PCr peak. A relaxation delay of 4 s between the last excitation pulse and beginning subsequent saturation period was kept constant. The peak intensities were obtained by fitting to a Lorentzian function using AMARES [60] from the jMRUI software (http://www.mrui.uab.es/mrui). The forward creatine kinase rate constant k_{for} and the apparent T_1 relaxation time of PCr during the γ-ATP saturation (T_{1sat}) were obtained from a nonlinear regression of relative PCr signal intensities $M(t_{sat})/M(0)$ as a function of t_{sat} according to the equation:

$$M(t_{sat})/M(0) = (1 - k_{for}T_{1sat}) + k_{for}T_{1sat}\exp(-t_{sat}/T_{1sat}).$$

The intracellular pH was calculated from the difference in chemical shifts of peaks of Pi and PCr using the equation [61]:

$$\mathrm{pHi} = 6.77 + \log(\delta\mathrm{Pi} - 3.29)/(5.68 - \delta\mathrm{Pi}),$$

where δPi is the chemical shift of the Pi resonance relative to PCr.

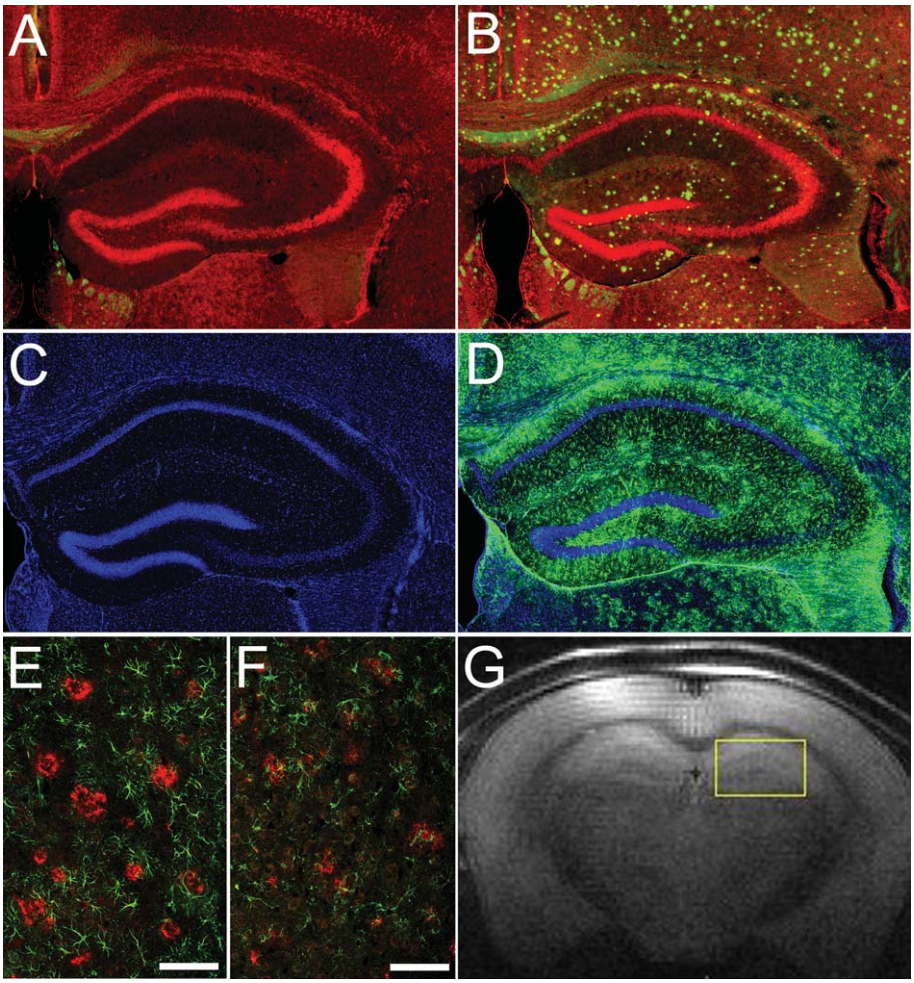

Fig. 1. Overview of the neuropathology in 39-week old 5xFAD mice at the level of the dorsal hippocampus. Amyloid pathology was revealed by Thioflavin S staining in wild-type (A) and transgenic (B) brain (Thioflavin S in green, ethidium bromide in red). The amyloid accumulation is associated with strong astrogliosis revealed by GFAP immunostaining in wild-type (C) and 5xFAD (D), GFAP staining in green, DAPI in blue. (E, F) Co-localization of reactive astrocytes and activated microglia with amyloid deposits in the neocortex as revealed by an immunostaining against amyloid-β peptide (in red) and either GFAP (E) or Iba1 (F) (in green). Scale bar = 100 μm. Localization of the volume of interest for proton MR spectroscopy is shown in (G).

Unpaired two-tailed Student's *t*-test was used to compare metabolite concentrations in the transgenic and wild-type mice. The error bars represent standard deviations.

Brain processing and histology

Animals were anaesthetized by intraperitoneal injection of pentobarbital (150 mg/kg) and transcardially perfused with cold phosphate buffered saline (PBS). Brains were extracted and fixed in paraformaldehyde 4% in PBS overnight at 4°C. Then brains were cryo-protected in a solution of PBS sucrose 25%(w/v), embedded in OCT compound, snap-froze and stored at −80°C until further processing. Coronal sections were performed using a cryostat (Leica CM3050S). Histology and immunohistochemistry were performed on 40-μm-thick free-floating sections. Thioflavin S staining was performed according to the following procedure: sections were washed twice in PBS (2 × 5 min), then incubated under agitation in a solution of Thioflavin S 0.01% (w/v) in ethanol 50% (v/v) during 8 min, followed by two baths in ethanol 50% (2 × 5 min) and PBS (2 × 10 min). Immunohistochemistry was performed with the following antibodies according to standard procedures: anti-amyloid-β (6E10, SIG-39320, Covance, 1/500), anti-GFAP (Z0334, Dako, 1/500), anti-Iba1 (019-19741, Wako, 1/100). Secondary antibodies: anti-mouse Cye3 (715-165-151, Jackson ImmunoResearch Laboratories, 1/1000) and anti-rabbit Alexa 488 (A21026, Invitrogen, 1/600). Sections were finally mounted in glycerol 80% and imaged with an epifluorescent microscope (LEICA DM5500).

RESULTS

As described by Oakley et al. [52], the 5xFAD model shows a very early onset of amyloid deposition (starting at 2 months in the subiculum and in the frontal cortex), a concomitant early inflammation and gliosis, and a synaptic loss as soon as 4 months of age. In this regard, this model presents a neuropathology similar to AD with the exception of the tau pathology, although the latter has not been fully investigated in this model [52, 62]. To determine if this model recapitulates the MR spectroscopic features of AD, a cohort of 5xFAD mice and wild-type littermates were studied at an advanced age between 8 and 10 months in a VOI covering the vast majority of the dorsal hippocampus (Fig. 1G). As shown in Fig. 1, numerous amyloid deposits were observed in transgenic animals at this age in the selected VOI (Fig. 1A, B). A strong astrogliosis was clearly observed in the same region (Fig. 1C, D) as well as a mild microglial response associated with amyloid deposits (Fig. 1E, F).

Figure 2 shows typical proton spectra measured in the hippocampal region of 5xFAD and wild-type mice. The high quality of spectra exhibiting excellent resolution and signal-to-noise enabled quantification of 18 metabolites. Comparison of the neurochemical profiles in dorsal hippocampus of the 5xFAD and wild-type mice is shown in Fig. 3, absolute metabolite concentrations and concentration ratios for most important metabolites are summarized in Table 2. At the age of 36 weeks, a statistically significant decrease in NAA, Glu, and glucose and a significant increase in the lactate concentration was found. At 40 and 44 weeks of age, changes typical for the human form of the disease, i.e., a decrease in NAA ($p < 0.004$) and an increase in myo-inositol ($p < 0.007$) were observed (Fig. 3, Table 2). In addition, the GABA concentration

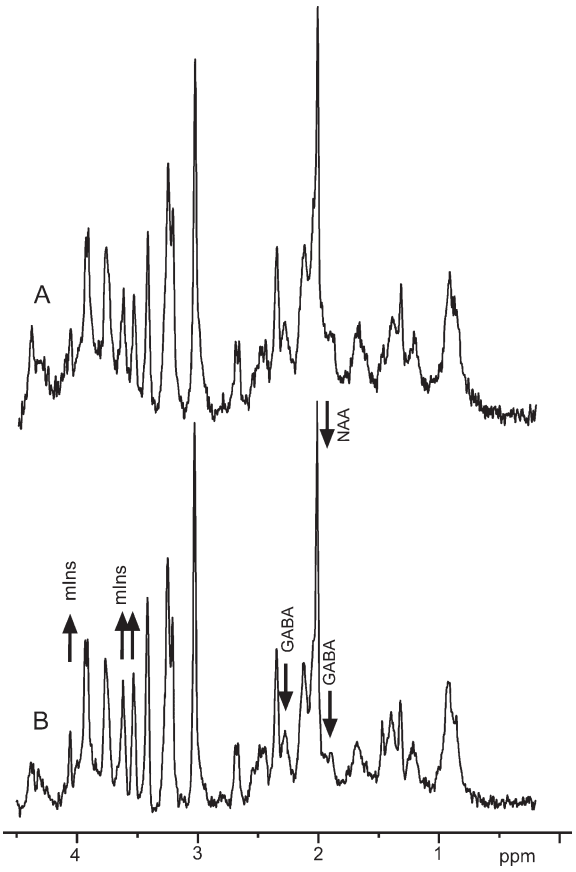

Fig. 2. Representative ^{1}H spectra measured in the dorsal hippocampus of a wild-type (A) and a 5xFAD mice (B).

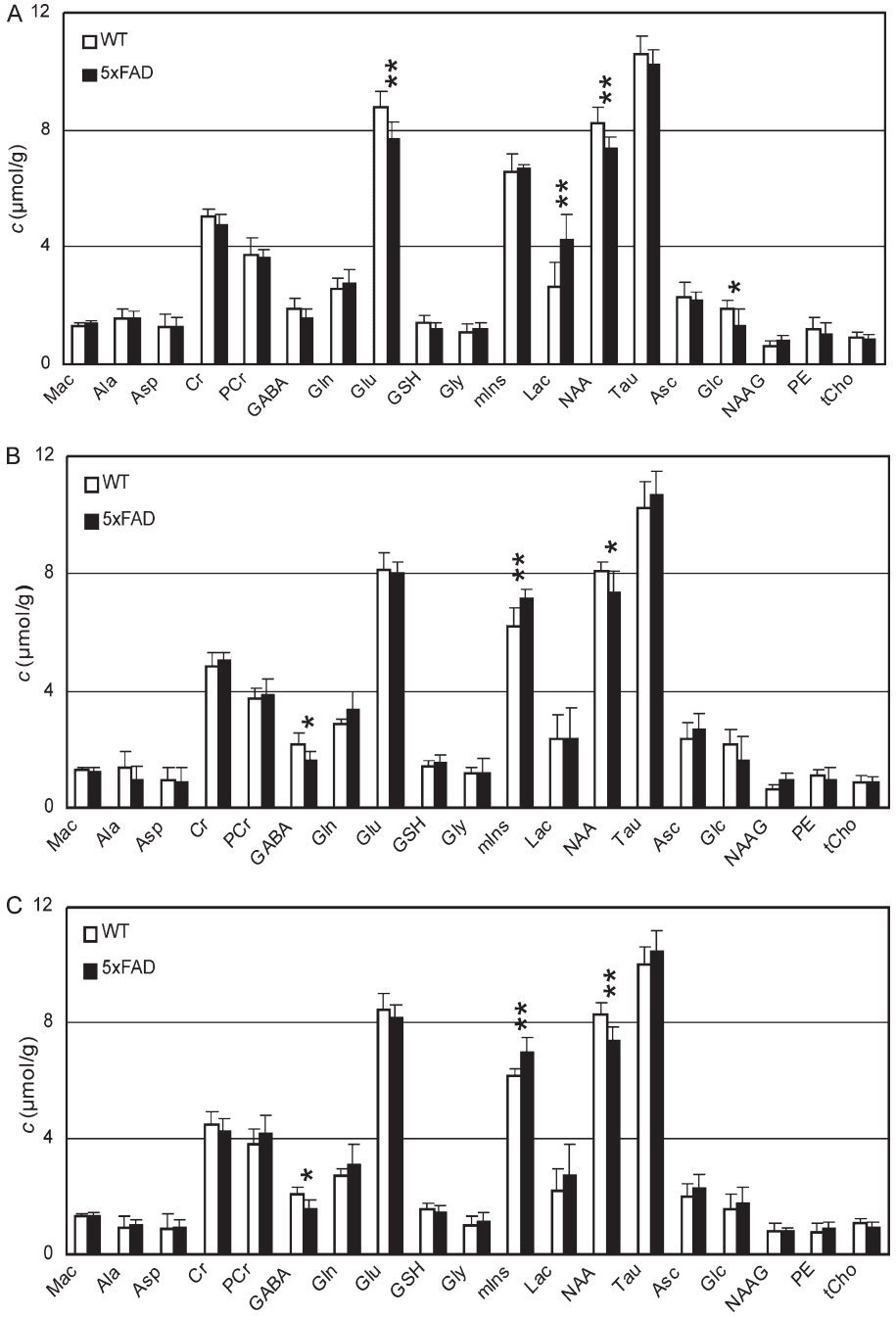

Fig. 3. Comparison of the neurochemical profile in dorsal hippocampus of the wild-type (WT) and 5xFAD mice at 36 (A), 40 (B), and 44 (C) weeks of age. Mac = macromolecules, Ala = alanine, Asp = aspartate, GSH = glutathione, Gly = glycine, Lac = lactate, Tau = taurine, Asc = ascorbate, Glc = glucose, NAAG = N-acetylaspartylglutamate, PE = phosphoethanolamine, tCho = total choline. Significantly different values are denoted by *($p < 0.05$) and **($p < 0.01$).

was also significantly decreased ($p < 0.015$) in the AD mice. The differences observed in the temporal part of hippocampus were similar, with higher p-values due to lower signal-to-noise ratio (data not shown).

In vivo ^{31}P spectra (Fig. 4) were also measured at 36 weeks of age from the volume of interest shown in Fig. 5. We observed a trend for an increase in the PCr/γ-ATP peak intensity ratio which however did not

Table 2
Concentrations of selected metabolites obtained from ^{1}H spectra, concentration ratios obtained from ^{31}P spectra and forward rate constants of the creatine kinase reaction in brain of wild-type (WT) and 5xFAD mice

Metabolite or metabolic ratio	^{1}H spectroscopy, c (μmol/g)					
	36 weeks		40 weeks		44 weeks	
	WT	5xFAD	WT	5xFAD	WT	5xFAD
Creatine	5.0 ± 0.2	4.8 ± 0.3	4.8 ± 0.4	5.0 ± 0.3	4.5 ± 0.5	4.3 ± 0.4
Phosphocreatine	3.8 ± 0.6	3.6 ± 0.3	3.8 ± 0.3	3.9 ± 0.6	3.8 ± 0.5	4.2 ± 0.6
γ-aminobutyrate	1.9 ± 0.3	1.6 ± 0.3	2.1 ± 0.4*	1.6 ± 0.3*	2.1 ± 0.3*	1.6 ± 0.3*
Glutamine	2.6 ± 0.3	2.8 ± 0.4	2.8 ± 0.2	3.4 ± 0.6	2.8 ± 0.3	3.1 ± 0.7
Glutamate	8.8 ± 0.6**	7.7 ± 0.6**	8.2 ± 0.5	8.0 ± 0.4	8.4 ± 0.6	8.2 ± 0.4
myo-inositol	6.6 ± 0.6	6.6 ± 0.2	6.2 ± 0.6**	7.2 ± 0.3**	6.2 ± 0.3**	7.0 ± 0.5**
N-acetylaspartate	8.2 ± 0.5**	7.4 ± 0.4**	8.1 ± 0.3*	7.4 ± 0.7*	8.3 ± 0.4**	7.4 ± 0.5**
Taurine	10.6 ± 0.6	10.2 ± 0.5	10.2 ± 0.9	10.7 ± 0.8	10.0 ± 0.6	10.5 ± 0.7
Phosphoethanolamine	1.2 ± 0.4	1.1 ± 0.4	1.1 ± 0.1	0.9 ± 0.5	0.7 ± 0.3	0.9 ± 0.2
Total choline	0.9 ± 0.2	0.8 ± 0.2	0.9 ± 0.2	0.9 ± 0.2	1.1 ± 0.2	0.9 ± 0.2
	^{31}P spectroscopy					
	36 weeks				72 weeks	
	WT	5xFAD			WT	5xFAD
$k_{PCr \longrightarrow ATP}$ (s^{-1})	0.45 ± 0.08	0.49 ± 0.06			0.49 ± 0.04	0.43 ± 0.06
Phosphocreatine/γ-ATP	1.4 ± 0.3	1.6 ± 0.4			1.4 ± 0.1	1.5 ± 0.2
Phosphocreatine/Inorganic phosphate	2.2 ± 0.7	2.0 ± 0.6				
Phosphomonoesters/γ-ATP	1.3 ± 0.3	1.2 ± 0.4				
Phosphodiesters/γ-ATP	0.24 ± 0.09	0.18 ± 0.09				

*Statistically significant $p < 0.05$.; **Statistically significant $p < 0.01$.

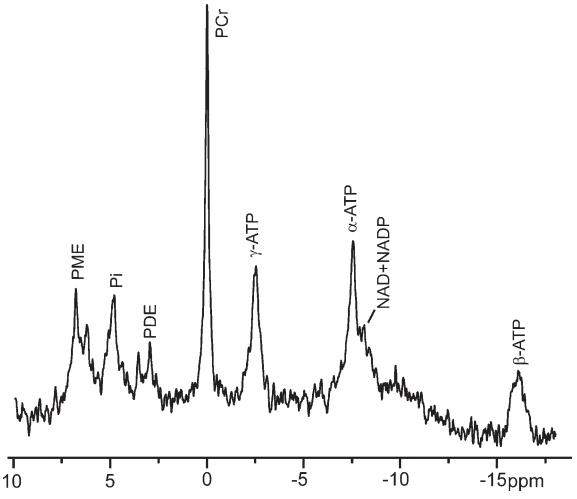

Fig. 4. ^{31}P spectrum of brain of an 5xFAD mouse.

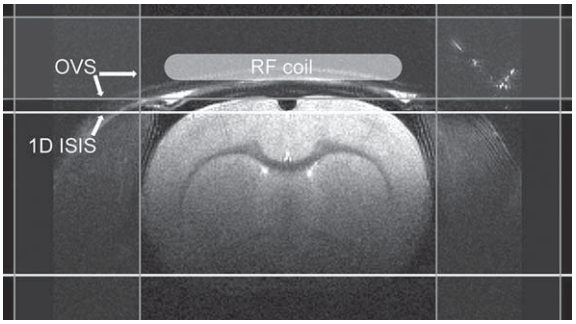

Fig. 5. Volume of interest selected for ^{31}P spectroscopy by outer volume saturation (OVS) and by one-dimensional ISIS localization (1D ISIS).

reach statistical significance ($p = 0.14$). There was also a non-significant trend for a decrease in PDE/ATP ratio ($p = 0.13$) in the transgenic mouse brain compared to wild-type controls. No differences ($p > 0.4$) in PCr/Pi and PME/γ-ATP were observed between transgenic and wild-type mice (Fig. 6, Table 2). In addition, the calculated values of the forward rate constant of the creatine kinase reaction k_{for} did not show any significant difference ($p = 0.2$). The measurement of k_{for} and PCr/γ-ATP was repeated in aged mice at 72 weeks of age. The values were similar to those obtained in younger animals and no significant difference between transgenic and wild-type mice was detected (Fig. 6, Table 2). The intracellular pHi in brain of the 36-week old transgenic and wild-type mice was the same within experimental error, 7.03 ± 0.02 and 7.02 ± 0.03, respectively.

DISCUSSION

As it was demonstrated in several reports, transgenic mouse models of AD can reproduce some neuropathological features of this disease. The typical neurochemical profile of AD is demonstrated by a

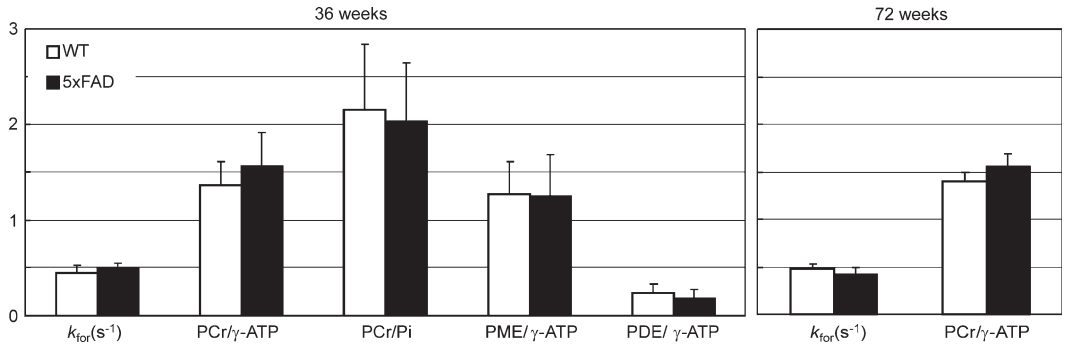

Fig. 6. Rate constant of the creatine kinase reaction k_{for} and metabolite peak intensity ratios in brain of young and aged wild-type and 5xFAD mice.

decrease in NAA and an increase in mIns concentrations. The lower level of NAA corresponding to reduction of neurons is consistently replicated in most studied transgenic models (Table 1). In contrast, most transgenic mouse models of AD do not show any mIns changes. One of them, AβPP$\times$PS1$_{M146L}$, even shows a decrease of mIns before the onset of the pathology (2.5 months) [35], although an increase is also reported at a later stage (20 months) [36]. These data suggest that the increase in mIns is only replicated when the pathology is severe. In agreement, our study on the 5xFAD mouse model, which presents a very fast development of the amyloid pathology, displays neurochemical changes typical for human AD patients much earlier, at about 9 months of age. Some authors suggest that mIns may even be an earlier marker than NAA for AD and other dementia [33, 63]. Thus, the early change in the mIns level observed in the studied 5xFAD mice may indicate closer similarity of this transgenic model with the human disease. In this regard, the AβPP$\times$PS1$_{\Delta E9}$ (line 85) mice measured by Chen et al. [40] might represent even a better model because it shows an increase in mIns earlier, at 3 months of age. However, since this increase in mIns appears before the onset of amyloid deposition in this model, it is unclear whether this phenomenon results from the pathology itself or from subtle effects of the transgenes during embryogenesis. Further studies at earlier time points will allow clarification of this point.

The decrease in the concentration of some neurotransmitters can also be related to neuronal death. We observed a significant decrease in GABA at 40 and 44 weeks of age and of Glu in the 36-week old AD mice relative to the wild-type ones. The GABA levels in brain of AD patients have not yet been reported due to difficulties in the detection of GABA peaks. However, improved spectral resolution and increased signal-to-noise of high-field human scanners would allow for quantification of metabolites such as GABA, Glu, and Gln, which may provide additional diagnostic information for AD.

The increase of lactate and decrease of glucose concentration in the 5xFAD mice at 36 weeks of age may be related to changes in animal physiology caused by anesthesia. Since no artificial ventilation was used and plasma glucose levels were not monitored during the experiments, these changes should be interpreted with care. In accordance with the AβPP/PS1 mice [36] but in contrast with the Tg2576 [33], no difference in the taurine concentration was found in the 5xFAD mice.

There is growing evidence that mitochondrial dysfunction associated with chronic oxidative stress can be a prominent and early event in AD and might explain selective degeneration of particular neuronal populations [64]. ^{31}P spectroscopy confirmed some findings of ^{1}H MRS experiments. Assuming constant concentration of ATP, the PCr level was unchanged in the 5xFAD mice, which is in accordance with observations in ^{1}H spectra (Fig. 3). The stable concentrations of PCr in the 5xFAD mice may indicate the absence of chronic hypoxia or ischemia in the brain tissue. The same conclusion can be drawn from the unchanged phosphorylation index PCr/Pi and pHi. The peaks of PME are mainly formed by phosphoethanolamine, which is also detected in ^{1}H spectra, and phosphorylcholine, which contributes to the ^{1}H total choline signal (Fig. 3). The PDE signal is mainly formed by glycerophosphorylcholine, which also contributes to the total choline peak in ^{1}H spectra. None of these peaks changed significantly in the 5xFAD mice. In addition, we did not observe any decrease in the rate constant of the creatine kinase reaction k_{for} even in elderly 5xFAD mice. These results suggest that energy supplies do not appear to be primarily affected in the brain of the 5xFAD mice,

whereas energy consumption might be depressed. This conclusion is supported by a previous finding that the creatine kinase rate constant decreases under chronic brain ischemia [65]. Further studies are needed to explore the role of impaired energy metabolism in the onset on AD pathogenesis and progression in humans as well as in transgenic AD models.

ACKNOWLEDGMENTS

This study was supported by the Center for Biomedical Imaging (CIBM) of the UNIL, UNIGE, HUG, CHUV, EPFL, the Leenaards and Jeantet Foundations, the EU grant No. MRTN-CT-2006-035801 (C.C.) and partially by the 7th Framework Programme of EC No. HEALTH-F2-2009-223524 (M.C.).

Authors' disclosures available online (http://www.j-alz.com/disclosures/view.php?id=1206).

REFERENCES

[1] Goate A, Chartier-Harlin MC, Mullan M, Brown J, Crawford F, Fidani L, Giuffra L, Haynes A, Irving N, James L, et al. (1991) Segregation of a missense mutation in the amyloid precursor protein gene with familial Alzheimer's disease. *Nature* **349**, 704-706.

[2] Rogaev EI, Sherrington R, Rogaeva EA, Levesque G, Ikeda M, Liang Y, Chi H, Lin C, Holman K, Tsuda T, et al. (1995) Familial Alzheimer's disease in kindreds with missense mutations in a gene on chromosome 1 related to the Alzheimer's disease type 3 gene. *Nature* **376**, 775-778.

[3] Sherrington R, Rogaev EI, Liang Y, Rogaeva EA, Levesque G, Ikeda M, Chi H, Lin C, Li G, Holman K, Tsuda T, Mar L, Foncin JF, Bruni AC, Montesi MP, Sorbi S, Rainero I, Pinessi L, Nee L, Chumakov I, Pollen D, Brookes A, Sanseau P, Polinsky RJ, Wasco W, Da Silva HA, Haines JL, Perkicak-Vance MA, Tanzi RE, Roses AD, Fraser PE, Rommens JM, St George-Hyslop PH (1995) Cloning of a gene bearing missense mutations in early-onset familial Alzheimer's disease. *Nature* **375**, 754-760.

[4] Hutton M, Lendon CL, Rizzu P, Baker M, Froelich S, Houlden H, Pickering-Brown S, Chakraverty S, Isaacs A, Grover A, Hackett J, Adamson J, Lincoln S, Dickson D, Davies P, Petersen RC, Stevens M, de Graaff E, Wauters E, van Baren J, Hillebrand M, Joosse M, Kwon JM, Nowotny P, Che LK, Norton J, Morris JC, Reed LA, Trojanowski J, Basun H, Lannfelt L, Neystat M, Fahn S, Dark F, Tannenberg T, Dodd PR, Hayward N, Kwok JB, Schofield PR, Andreadis A, Snowden J, Craufurd D, Neary D, Owen F, Oostra BA, Hardy J, Goate A, van Swieten J, Mann D, Lynch T, Heutink P (1998) Association of missense and 5′-splice-site mutations in tau with the inherited dementia FTDP-17. *Nature* **393**, 702-705.

[5] Hall AM, Roberson ED (2011) Mouse models of Alzheimer's disease. *Brain Res Bull*, doi:10.1016/j.brainresbull.2011.1011.1017

[6] Oddo S, Caccamo A, Shepherd JD, Murphy MP, Golde TE, Kayed R, Metherate R, Mattson MP, Akbari Y, LaFerla FM (2003) Triple-transgenic model of Alzheimer's disease with plaques and tangles: Intracellular Aβ and synaptic dysfunction. *Neuron* **39**, 409-421.

[7] Grueninger F, Bohrmann B, Czech C, Ballard TM, Frey JR, Weidensteiner C, von Kienlin M, Ozmen L (2010) Phosphorylation of Tau at S422 is enhanced by Aβ in TauPS2APP triple transgenic mice. *Neurobiol Dis* **37**, 294-306.

[8] Eriksen JL, Janus CG (2007) Plaques, tangles, and memory loss in mouse models of neurodegeneration. *Behav Genet* **37**, 79-100.

[9] Morrissette DA, Parachikova A, Green KN, LaFerla FM (2009) Relevance of transgenic mouse models to human Alzheimer disease. *J Biol Chem* **284**, 6033-6037.

[10] Mandal PK (2007) Magnetic resonance spectroscopy (MRS) and its application in Alzheimer's disease. *Concepts Magn Reson A* **30A**, 40-64.

[11] Mandal PK, Akolkar H (2011) A new experimental approach and signal processing scheme for the detection and quantitation of ^{31}P brain neurochemicals from *in vivo* MRS studies using dual tuned (^{1}H/^{31}P) head coil. *Biochem Biophys Res Commun* **412**, 302-306.

[12] Yesavage JA, O'Hara R, Kraemer H, Noda A, Taylor JL, Ferris S, Gely-Nargeot MC, Rosen A, Friedman L, Sheikh J, Derouesne C (2002) Modeling the prevalence and incidence of Alzheimer's disease and mild cognitive impairment. *J Psychiatr Res* **36**, 281-286.

[13] Doraiswamy PM, Charles HC, Krishnan KR (1998) Prediction of cognitive decline in early Alzheimer's disease. *Lancet* **352**, 1678.

[14] Jessen F, Gur O, Block W, Ende G, Frolich L, Hammen T, Wiltfang J, Kucinski T, Jahn H, Heun R, Maier W, Kolsch H, Kornhuber J, Traber F (2009) A multicenter ^{1}H-MRS study of the medial temporal lobe in AD and MCI. *Neurology* **72**, 1735-1740.

[15] Miller BL, Moats RA, Shonk T, Ernst T, Woolley S, Ross BD (1993) Alzheimer disease: Depiction of increased cerebral myo-inositol with proton MR spectroscopy. *Radiology* **187**, 433-437.

[16] Moats RA, Ernst T, Shonk TK, Ross BD (1994) Abnormal cerebral metabolite concentrations in patients with probable Alzheimer disease. *Magn Reson Med* **32**, 110-115.

[17] Schuff N, Amend DL, Meyerhoff DJ, Tanabe JL, Norman D, Fein G, Weiner MW (1998) Alzheimer disease: Quantitative H-1 MR spectroscopic imaging of frontoparietal brain. *Radiology* **207**, 91-102.

[18] Klunk WE, Panchalingam K, Moossy J, McClure RJ, Pettegrew JW (1992) N-acetyl-L-aspartate and other amino acid metabolites in Alzheimer's disease brain: A preliminary proton nuclear magnetic resonance study. *Neurology* **42**, 1578-1585.

[19] Schuff N, Amend D, Ezekiel F, Steinman SK, Tanabe J, Norman D, Jagust W, Kramer JH, Mastrianni JA, Fein G, Weiner MW (1997) Changes of hippocampal N-acetyl aspartate and volume in Alzheimer's disease. A proton MR spectroscopic imaging and MRI study. *Neurology* **49**, 1513-1521.

[20] Huang W, Alexander GE, Chang L, Shetty HU, Krasuski JS, Rapoport SI, Schapiro MB (2001) Brain metabolite concentration and dementia severity in Alzheimer's disease: A ^{1}H MRS study. *Neurology* **57**, 626-632.

[21] Kantarci K, Petersen RC, Boeve BF, Knopman DS, Tang-Wai DF, O'Brien PC, Weigand SD, Edland SD, Smith GE, Ivnik RJ, Ferman TJ, Tangalos EG, Jack CR Jr (2004) ^{1}H MR spectroscopy in common dementias. *Neurology* **63**, 1393-1398.

[22] Pfefferbaum A, Adalsteinsson E, Spielman D, Sullivan EV, Lim KO (1999) *In vivo* spectroscopic quantification of the N-acetyl moiety, creatine, and choline from large volumes of brain gray and white matter: Effects of normal aging. *Magn Reson Med* **41**, 276-284.

[23] Chantal S, Labelle M, Bouchard RW, Braun CM, Boulanger Y (2002) Correlation of regional proton magnetic resonance spectroscopic metabolic changes with cognitive deficits in mild Alzheimer disease. *Arch Neurol* **59**, 955-962.

[24] Watanabe T, Shiino A, Akiguchi I (2010) Absolute quantification in proton magnetic resonance spectroscopy is useful to differentiate amnesic mild cognitive impairment from Alzheimer's disease and healthy aging. *Dement Geriatr Cogn Disord* **30**, 71-77.

[25] Ackl N, Ising M, Schreiber YA, Atiya M, Sonntag A, Auer DP (2005) Hippocampal metabolic abnormalities in mild cognitive impairment and Alzheimer's disease. *Neurosci Lett* **384**, 23-28.

[26] Wang ZQ, Zhao C, Yu L, Zhou WD, Li KC (2009) Regional metabolic changes in the hippocampus and posterior cingulate area detected with 3-Tesla magnetic resonance spectroscopy in patients with mild cognitive impairment and Alzheimer disease. *Acta Radiol* **50**, 312-319.

[27] Rupsingh R, Borrie M, Smith M, Wells JL, Bartha R (2011) Reduced hippocampal glutamate in Alzheimer disease. *Neurobiol Aging* **32**, 802-810.

[28] Adalsteinsson E, Sullivan EV, Kleinhans N, Spielman DM, Pfefferbaum A (2000) Longitudinal decline of the neuronal marker N-acetyl aspartate in Alzheimer's disease. *Lancet* **355**, 1696-1697.

[29] Ernst T, Chang L, Melchor R, Mehringer CM (1997) Frontotemporal dementia and early Alzheimer disease: Differentiation with frontal lobe H-1 MR spectroscopy. *Radiology* **203**, 829-836.

[30] Antuono PG, Jones JL, Wang Y, Li SJ (2001) Decreased glutamate + glutamine in Alzheimer's disease detected *in vivo* with ^{1}H-MRS at 0.5 T. *Neurology* **56**, 737-742.

[31] Kara F, Braakman N, van Buchem MA, de Groot HJM, Alia A (2011) Prospects of magnetic resonance spectroscopy in mouse models of Alzheimer's disease. *Curr Med Imaging Rev* **7**, 80-87.

[32] Hsiao K, Chapman P, Nilsen S, Eckman C, Harigaya Y, Younkin S, Yang F, Cole G (1996) Correlative memory deficits, Aβ elevation, and amyloid plaques in transgenic mice. *Science* **274**, 99-102.

[33] Dedeoglu A, Choi JK, Cormier K, Kowall NW, Jenkins BG (2004) Magnetic resonance spectroscopic analysis of Alzheimer's disease mouse brain that express mutant human APP shows altered neurochemical profile. *Brain Res* **1012**, 60-65.

[34] Holcomb L, Gordon MN, McGowan E, Yu X, Benkovic S, Jantzen P, Wright K, Saad I, Mueller R, Morgan D, Sanders S, Zehr C, O'Campo K, Hardy J, Prada CM, Eckman C, Younkin S, Hsiao K, Duff K (1998) Accelerated Alzheimer-type phenotype in transgenic mice carrying both mutant amyloid precursor protein and presenilin 1 transgenes. *Nat Med* **4**, 97-100.

[35] Oberg J, Spenger C, Wang FH, Andersson A, Westman E, Skoglund P, Sunnemark D, Norinder U, Klason T, Wahlund LO, Lindberg M (2008) Age related changes in brain metabolites observed by ^{1}H MRS in APP/PS1 mice. *Neurobiol Aging* **29**, 1423-1433.

[36] Marjanska M, Curran GL, Wengenack TM, Henry PG, Bliss RL, Poduslo JF, Jack CR Jr, Ugurbil K, Garwood M (2005) Monitoring disease progression in transgenic mouse models of Alzheimer's disease with proton magnetic resonance spectroscopy. *Proc Natl Acad Sci U S A* **102**, 11906-11910.

[37] Jack CR Jr, Marjanska M, Wengenack TM, Reyes DA, Curran GL, Lin J, Preboske GM, Poduslo JF, Garwood M (2007) Magnetic resonance imaging of Alzheimer's pathology in the brains of living transgenic mice: A new tool in Alzheimer's disease research. *Neuroscientist* **13**, 38-48.

[38] Choi JK, Jenkins BG, Carreras I, Kaymakcalan S, Cormier K, Kowall NW, Dedeoglu A (2010) Anti-inflammatory treatment in AD mice protects against neuronal pathology. *Exp Neurol* **223**, 377-384.

[39] McGowan E, Sanders S, Iwatsubo T, Takeuchi A, Saido T, Zehr C, Yu X, Uljon S, Wang R, Mann D, Dickson D, Duff K (1999) Amyloid phenotype characterization of transgenic mice overexpressing both mutant amyloid precursor protein and mutant presenilin 1 transgenes. *Neurobiol Dis* **6**, 231-244.

[40] Chen SQ, Wang PJ, Ten GJ, Zhan W, Li MH, Zang FC (2009) Role of myo-inositol by magnetic resonance spectroscopy in early diagnosis of Alzheimer's disease in APP/PS1 transgenic mice. *Dement Geriatr Cogn Disord* **28**, 558-566.

[41] Jankowsky JL, Slunt HH, Ratovitski T, Jenkins NA, Copeland NG, Borchelt DR (2001) Co-expression of multiple transgenes in mouse CNS: A comparison of strategies. *Biomol Eng* **17**, 157-165.

[42] Jankowsky JL, Fadale DJ, Anderson J, Xu GM, Gonzales V, Jenkins NA, Copeland NG, Lee MK, Younkin LH, Wagner SL, Younkin SG, Borchelt DR (2004) Mutant presenilins specifically elevate the levels of the 42 residue β-amyloid peptide *in vivo*: Evidence for augmentation of a 42-specific γ secretase. *Hum Mol Genet* **13**, 159-170.

[43] Garcia-Alloza M, Robbins EM, Zhang-Nunes SX, Purcell SM, Betensky RA, Raju S, Prada C, Greenberg SM, Bacskai BJ, Frosch MP (2006) Characterization of amyloid deposition in the APPswe/PS1dE9 mouse model of Alzheimer disease. *Neurobiol Dis* **24**, 516-524.

[44] Burgess BL, McIsaac SA, Naus KE, Chan JY, Tansley GH, Yang J, Miao F, Ross CJ, van Eck M, Hayden MR, van Nostrand W, St George-Hyslop P, Westaway D, Wellington CL (2006) Elevated plasma triglyceride levels precede amyloid deposition in Alzheimer's disease mouse models with abundant Aβ in plasma. *Neurobiol Dis* **24**, 114-127.

[45] Richards JG, Higgins GA, Ouagazzal AM, Ozmen L, Kew JN, Bohrmann B, Malherbe P, Brockhaus M, Loetscher H, Czech C, Huber G, Bluethmann H, Jacobsen H, Kemp JA (2003) PS2APP transgenic mice, coexpressing hPS2mut and hAPPswe, show age-related cognitive deficits associated with discrete brain amyloid deposition and inflammation. *J Neurosci* **23**, 8989-9003.

[46] von Kienlin M, Kunnecke B, Metzger F, Steiner G, Richards JG, Ozmen L, Jacobsen H, Loetscher H (2005) Altered metabolic profile in the frontal cortex of PS2APP transgenic mice, monitored throughout their life span. *Neurobiol Dis* **18**, 32-39.

[47] Kim J, Lee S-P, Michaelis ML, Choi I-Y (2009) Detecting progression of Alzheimer's disease pathology in the triple transgenic mouse brain using ^{1}H MRS. In: *Proc ISMRM 17th Scientific Meeting & Exhibition*. International Society for Magnetic Resonance in Medicine, Honolulu, USA, p. 3302.

[48] Choi JK, Dedeoglu A, Jenkins BG (2007) Application of MRS to mouse models of neurodegenerative illness. *NMR Biomed* **20**, 216-237.

[49] Santacruz K, Lewis J, Spires T, Paulson J, Kotilinek L, Ingelsson M, Guimaraes A, DeTure M, Ramsden M, McGowan E, Forster C, Yue M, Orne J, Janus C, Mariash A, Kuskowski M, Hyman B, Hutton M, Ashe KH (2005) Tau suppression in a neurodegenerative mouse model improves memory function. *Science* **309**, 476-481.

[50] Kim J, Choi I-Y, Duff K, Lee P (2011) Neurochemical changes in olfactory system and hippocampus regions of Tau transgenic mice using ^{1}H MRS. In: *Proc ISMRM 19th Scientific*

Meeting & Exhibition. International Society for Magnetic Resonance in Medicine, Montreal, p. 2251.

[51] Yang D, Xie Z, Stephenson D, Morton D, Hicks CD, Brown TM, Sriram R, O'Neill S, Raunig D, Bocan T (2011) Volumetric MRI and MRS provide sensitive measures of Alzheimer's disease neuropathology in inducible Tau transgenic mice (rTg4510). *Neuroimage* **54**, 2652-2658.

[52] Oakley H, Cole SL, Logan S, Maus E, Shao P, Craft J, Guillozet-Bongaarts A, Ohno M, Disterhoft J, Van Eldik L, Berry R, Vassar R (2006) Intraneuronal β-amyloid aggregates, neurodegeneration, and neuron loss in transgenic mice with five familial Alzheimer's disease mutations: Potential factors in amyloid plaque formation. *J Neurosci* **26**, 10129-10140.

[53] Gruetter R, Tkáč I (2000) Field mapping without reference scan using asymmetric echo-planar techniques. *Magn Reson Med* **43**, 319-323.

[54] Mlynárik V, Gambarota G, Frenkel H, Gruetter R (2006) Localized short-echo-time proton MR spectroscopy with full signal-intensity acquisition. *Magn Reson Med* **56**, 965-970.

[55] Tkáč I, Starčuk Z, Choi IY, Gruetter R (1999) *In vivo* ^{1}H NMR spectroscopy of rat brain at 1ms echo time. *Magn Reson Med* **41**, 649-656.

[56] Provencher SW (1993) Estimation of metabolite concentrations from localized *in vivo* proton NMR spectra. *Magn Reson Med* **30**, 672-679.

[57] Mlynárik V, Cudalbu C, Xin L, Gruetter R (2008) ^{1}H NMR spectroscopy of rat brain *in vivo* at 14.1Tesla: Improvements in quantification of the neurochemical profile. *J Magn Reson* **194**, 163-168.

[58] Ordidge RJ, Connelly A, Lohman JAB (1986) Image-selected *in vivo* spectroscopy (ISIS) – a new technique for spatially selective NMR-spectroscopy. *J Magn Reson* **66**, 283-294.

[59] Luo Y, de Graaf RA, DelaBarre L, Tannus A, Garwood M (2001) BISTRO: An outer-volume suppression method that tolerates RF field inhomogeneity. *Magn Reson Med* **45**, 1095-1102.

[60] Vanhamme L, van den Boogaart A, Van Huffel S (1997) Improved method for accurate and efficient quantification of MRS data with use of prior knowledge. *J Magn Reson* **129**, 35-43.

[61] Petroff OAC, Prichard JW, Behar KL, Alger JR, Denhollander JA, Shulman RG (1985) Cerebral intracellular pH by ^{31}P nuclear magnetic resonance spectroscopy. *Neurology* **35**, 781-788.

[62] Jawhar S, Trawicka A, Jenneckens C, Bayer TA, Wirths O (2010) Motor deficits, neuron loss, and reduced anxiety coinciding with axonal degeneration and intraneuronal Aβ aggregation in the 5xFAD mouse model of Alzheimer's disease. *Neurobiol Aging* **33**, 196.e29-196.e40.

[63] Shonk T, Ross BD (1995) Role of increased cerebral myo-inositol in the dementia of Down syndrome. *Magn Reson Med* **33**, 858-861.

[64] Schmitt K, Grimm A, Kazmierczak A, Strosznajder JB, Gotz J, Eckert A (2011) Insights into mitochondrial dysfunction: Aging, amyloid-β and tau – a deleterious trio. *Antioxid Redox Signal*, doi:10.1089/ars.2011.4400

[65] Mlynárik V, Kašparová S, Liptaj T, Dobrota D, Horecký J, Belan V (1998) Creatine kinase reaction rates in rat brain during chronic ischemia. *Magn Reson Mater Phys* **7**, 162-165.

[66] Kawarabayashi T, Younkin LH, Saido TC, Shoji M, Ashe KH, Younkin SG (2001) Age-dependent changes in brain, CSF, and plasma amyloid β protein in the Tg2576 transgenic mouse model of Alzheimer's disease. *J Neurosci* **21**, 372-381.

[67] Sasaki A, Shoji M, Harigaya Y, Kawarabayashi T, Ikeda M, Naito M, Matsubara E, Abe K, Nakazato Y (2002) Amyloid cored plaques in Tg2576 transgenic mice are characterized by giant plaques, slightly activated microglia, and the lack of paired helical filament-typed, dystrophic neurites. *Virchows Arch* **441**, 358-367.

[68] Gordon MN, Holcomb LA, Jantzen PT, DiCarlo G, Wilcock D, Boyett KW, Connor K, Melachrino J, O'Callaghan JP, Morgan D (2002) Time course of the development of Alzheimer-like pathology in the doubly transgenic PS1+APP mouse. *Exp Neurol* **173**, 183-195.